Article | Received 27 April 2026; Revised 9 June 2026; Accepted 30 June 2026; Published 8 July 2026
https://doi.org/10.55092/ae20260005

Adaptive asymptotic tracking control for active suspension systems: an event-triggered approach with input saturation

Yingjie Deng[1,2], Fangcheng Liu[2,*], Xiangyu Meng[3], Yuxin Wu[3], Dingxuan Zhao[1,2], Tao Ni[3] and Namkyun Im[4]

[1] State Key Laboratory of Crane Technology, Yanshan University, Qinhuangdao, China
[2] School of Mechanical Engineering, Yanshan University, Qinhuangdao, China
[3] School of Vehicle and Energy, Yanshan University, Qinhuangdao, China
[4] Division of Navigation, Mokpo National Maritime University, Mokpo, Republic of Korea

* Correspondence author; E-mail: lfc@stumail.ysu.edu.cn.

Highlights:

- A novel asymptotic tracking method is proposed for active suspension systems with unknown road information to guarantee error convergence and high control accuracy.
- Auxiliary system theory is integrated to handle actuator saturation, improving the practicality and versatility of the control scheme.
- Combined with minimal learning parameters and event-triggered control, the designed method requires only one parameter update, which reduces computation cost and saves communication resources.

Abstract: In this paper, an adaptive neural asymptotic tracking control scheme with the event-triggered mechanism is presented for a quarter-car active suspension system (ASS) with unknown road inputs and input saturation. In the control design, an auxiliary system is constructed to compensate for the input saturation of the actuator, and a linear filter is introduced to solve the chattering problem of the suspension system under the zero dynamics. By integrating integral-bounded functions into the adaptive law and control law, asymptotic convergence of the tracking error is achieved with high precision. Using the adaptive backstepping control method and introducing the command filter, an event-triggered adaptive neural asymptotic tracking control algorithm is developed, in which the radial basis function neural networks (RBFNNs) are used to approximate the unknown model dynamics. Considering the waste of communication resources in the controller, the event-triggered control (ETC) law in the controller-to-actuator channel is designed. Benefiting from the minimal learning parameters (MLP) technique, the proposed scheme requires updating only one parameter, which reduces computational complexity and saves communication resources. By using the Lyapunov's method and the Barbalat's lemma, the asymptotic stability of the closed-loop system is proved, and the constraint conditions for vehicle ride comfort are also guaranteed. Finally, the effectiveness of the proposed method is further verified through simulations and experimental results.

Keywords: active suspension system (ASS); asymptotic tracking; event-triggered control (ETC); neural networks (NNs); input saturation; minimum learning parameter (MLP)

1. Introduction

In the past few decades, suspension systems have attracted great attention for its competence in improving vehicle handling stability and ride comfort. Suspension systems, as an important part connecting the vehicle body and axles, transmitting the forces acting between the wheels and the frame, not only buffering the impact of the rough road surface on the vehicle body, but also attenuating the resulting vibration. Compared to traditional semi-active suspensions and passive suspensions, active suspensions can regulate the output of the suspension actuator in real-time according to the movement of the body, and thereby show the better ride comfort [1].

There are many control methods proposed by scholars to enhance the control performance of active suspension system (ASS) in recent years, for example, active disturbance rejection control [2–4], model predictive control [5–7], sliding mode control [8–10], *etc.* The sprung mass changes with load, and the system parameters are uncertain and time-varying. These factors motivate the successful application of adaptive backstepping control to ASS. Pang *et al.* [11] solved the actuator input delay and finite time tracking problems using adaptive backstepping control. Sun *et al.* [12] investigated an active suspension fourth-order system by introducing a fuzzy logic system in the adaptive backstepping control. By considering the parameter uncertainty of the mechanical elastic wheel, an adaptive backstepping control with grey signal predictor is proposed [13]. However, the above backstepping control is susceptible to the problem of differential explosion for a complex system with nonlinear dynamics and the high order, such that the controller becomes more complex and detrimental to system stability. In order to solve the differential explosion problem, dynamic surface control (DSC) [14–16] and command filters [17–19] have been proposed. DSC replaces the differentiation of virtual control laws with a first-order filter. This technique has been extensively employed in underactuated ships [20,21] and unmanned aerial vehicles (UAVs) [22,23]. However, such filter-based substitution inevitably introduces differentiation errors. In contrast, command filters can not only produce the derivatives of virtual control laws, but also facilitate the design of error compensation signals. Therefore, this disposal is more consummate in mathematical explanation and practical application.

As the unknown nonlinearities exist in various mechanical systems, neural networks (NNs) have been widely used to address the nonlinear part [24–26]. The adaptive neural backstepping control is constructed to solve the problem of nonlinear dynamics with practical hydraulic actuator saturation and additive stochastic terms. Zhao *et al.* [27] developed a neural network observer by optimizing the control parameters using the particle swarm optimization approach, which attenuated vertical vibrations caused by road surface unevenness. The nonlinearities of the suspension system under deterministic road disturbance are eliminated by using radial basis function (RBF) neural network as part of the adaptive feedback linearization control law. However, the selection of basis functions in RBF NNs directly affects their control performance, and input saturation inevitably restricts the control signal in various active suspension systems, particularly in heavy vehicles. The saturation will result in the instability of the system and

the deteriorated control performance [28]. In order to address this problem, non-smooth saturated input problem is considered by using the idea of smooth hyperbolic function instead of saturated function, and the median theorem can ensure that the error is globally bounded. Wang *et al.* [24] compensated for the input saturation constraint by constructing a second-order auxiliary system. A saturation adaptive tracking controller was proposed [29]. An anti-windup method consisting of two filters was proposed [30]. Although actuator saturation is addressed in the above paper, it can only achieve uniformly ultimately bounded tracking errors, which is incapable of high tracking precision. Compared with the bounded results, the asymptotic tracking error is more preferred for its high-precision performance. Nevertheless in the ASS, the asymptotic stability is difficult to be obtained with input saturation. Therefore, how to achieve asymptotic stability tracking performance in ASS is a topic worth studying.

Due to the waste of communication resources caused by traditional continuous control, event-triggered control (ETC) has won significant attention in the context of network communication. Therefore, has won significant attention in the context of network communication *etc.* This control method performs intermittent sampling of signals, which can reduce computational costs and controller actions, and is an effective and fast control method without affecting control performance. Wang *et al.* [31] proposed a new event-triggered controller in the form of linear matrix inequality based on the improved relaxation inequality and extended Lyapunov-Krasovskii generalization. Ge *et al.* [32] designed an efficient dynamic event-triggered schedule and control cooperative design method for signal transmission delays and data loss, which can ensure the suspension performance as well as alleviate the resource consumption of controller area network (CAN). Deng *et al.* [33] proposed an event-triggered adaptive fuzzy optimal control strategy, which can reduce the consumption of communication resources in both actuator-to-controller and sensor-to-controller channels. In [34], a game-based ETC strategy is applied to the sensor-to-controller (SC) channel.

Motivated by the above inspiration, this paper investigates the high precision control of ASS with input saturation. By introducing the command filter, the adaptive backstepping control law is recursively designed to effectively avoid the differential explosion problem. By constituting the second-order auxiliary system, the actuator input saturation constraint can be released. A linear filter is constructed to reduce the vibration of the suspension under zero dynamics. The RBF NNs are used to approximate the dynamic uncertainties. According to the advantages of minimum learning parameters (MLP), asymptotic tracking performance is ensured by integrating the integral-bounded functions into the adaptive law and the control law. The use of ETC reduces the consumption of communication resources. It is better suited to the situation where communication is limited in practice. Compared to previous works, the contributions of this paper are mainly threefold:

(1) A novel asymptotic tracking method is proposed for the ASS with unknown road information. Compared with studies [24–27], the proposed scheme can achieve asymptotic convergence of the control error with the higher control accuracy.

(2) This article integrates auxiliary system theory with asymptotic stability to address the input saturation problem of actuators. Compared with studies [31,32,35], the proposed strategy has better practicality and versatility, making it applicable to a wider range of scenarios.

(3) Leveraging the strengths of MLP and ETC theory, the asymptotic tracking control method that we designed only requires updating one parameter. Compared with studies [17,24,28–30], our

proposed scheme not only effectively reduces computational complexity but also conserves communication resources, delivering enhanced resource efficiency.

2. Problem formulations and preliminaries

2.1. The model of quarter-car active suspension system

In this work, a quarter-car ASS is taken into consideration from [24], as shown in Figure 1. The kinetic equations of a quarter-car ASS is defined as:

$$\begin{cases} m_b\ddot{z}_s + f_t + f_v - u_m = 0 \\ m_u\ddot{z}_u - f_t - f_v + f_w + f_r + u_m = 0 \end{cases} \tag{1}$$

where z_s and z_u denote the displacement of the sprung and the unsprung of masses. z_r is the terrain height displacement, respectively. m_b and m_u denote the sprung mass and the unsprung mass. u_m is saturation control signal of the actuator. The suspension system stiffness f_t is described by $f_t(z_s - z_u) = k_a(z_s - z_u) + \gamma k_a(z_s - z_u)^3$, k_a represent the linear spring coefficient, and γ stands for the nonlinear suspension stiffness. The suspension damping is defined as $f_v = c_a(\dot{z}_s - \dot{z}_u) - c_b|\dot{z}_s - \dot{z}_u| + c_c\sqrt{|\dot{z}_s - \dot{z}_u|}\text{sgn}(\dot{z}_s - \dot{z}_u)$. The wheel stiffness and damping are defined as $f_w = k_t(z_u - z_r)$, $f_r = c_t(\dot{z}_u - \dot{z}_r)$. The positive constants c_t and k_t stand for the damping coefficient and linear spring coefficient of the tire. c_a represents the suspension damping coefficient, respectively. The positive constants c_b and c_c denote the nonlinear suspension damping coefficients.

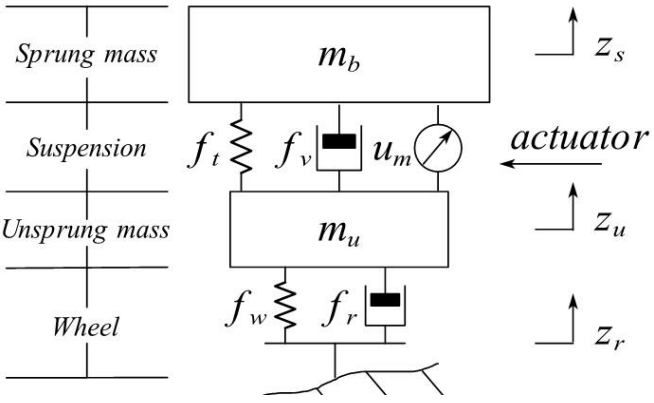

Figure 1. The structure of the quarter-car ASS.

In kinetic Equation (1), the actuator output is constrained by its physical and mechanical limitations. The assumption in the paper is a constant $\bar{u}_m > 0$ for the maximum value. When the absolute value of the output of the control signal goes above $\bar{u}_m$, the saturation appears. The saturation control signal u_m satisfies

$$u_m = \begin{cases} \bar{u}_m, & u > \bar{u}_m \\ u, & -\bar{u}_m \le u \le \bar{u}_m \\ -\bar{u}_m, & u < -\bar{u}_m \end{cases}. \tag{2}$$

where u is the designed control law.

Choosing the following state variables: $x_1 = z_s$, $x_2 = \dot{z}_s$, $x_3 = z_u$ and $x_4 = \dot{z}_u$. Then, the Equation (1) is translated into the Equation (3) based on the defined new stable variables:

$$\begin{cases} \dot{x}_1 = x_2 \\ \dot{x}_2 = \dfrac{1}{m_b}\left(-f_t - f_v + u_m\right) \\ \dot{x}_3 = x_4 \\ \dot{x}_4 = \dfrac{1}{m_u}\left(f_t + f_v - f_w - f_r - u_m\right) \end{cases} \tag{3}$$

The simplified vehicle-body dynamics (Equation (4)) facilitate later development analysis

$$\dot{x}_2 = h(x) + \kappa u_m \tag{4}$$

where $h(x) = -(f_t + f_v)/m_b$, $\kappa = 1/m_b$.

During the operation of the vehicle, the number of cargoes and passengers change randomly, which lead to a change in the mass of the body m_b. In addition, the load-bearing capacity of the vehicle is limited. So, κ and the function $h(x)$ are the unknown bounded.

Control Objective: Consider a quarter-car ASS in Equation (1) with input saturation, the control objective of this article is to design an event-triggered adaptive neural asymptotic tracking control input u_m such that x_1 can track the filter signal of x_3 asymptotically with less control energy.

2.2. Preliminaries

There are some useful mathematical tools are introduced here, which are described below.

Assumption 1: Since the active suspension works in the limited space with the limited efficiency, the variables in Equations (1) and (3) are defined in a compact set.

Lemma 1 [14]: If $\bar{x}$ is in a compact set, then the nonlinear function $f(\bar{x})$ is depicted by a radial basis function NN as

$$f(\bar{x}) = W^{\mathrm{T}}\varphi(\bar{x}) + \varepsilon(\bar{x}) \tag{5}$$

where $f(\bar{x}) \in \mathscr{R}^n$, $W \in \mathscr{R}^m$ and $\varphi(\bar{x}) \in \mathscr{R}^m$. W and $\varphi(\bar{x})$ represent the neural weight vector and the neural basis function vector, respectively. $\varepsilon(\bar{x})$ is the estimation error with the bound of $|\varepsilon(\bar{x})| \leq \bar{\varepsilon}$, $\bar{\varepsilon} > 0$. By the proper choice of W and $\varphi(\bar{x})$, $\bar{\varepsilon}$ can be varied to an arbitrarily small value.

Lemma 2 [36]: $\varphi(\bar{x})$ can be chosen as Gaussian functions. If $\bar{x} = [x_1, \cdots, x_m]^{\mathrm{T}}$ and $\bar{x}_p = [x_1, \cdots, x_n]^{\mathrm{T}}$, where $n \leq m$, then the inequality applies

$$\|\varphi(\bar{x})\| \leq \|\varphi(\bar{x}_p)\| \tag{6}$$

Lemma 3 [37]: For arbitrary variable s and a continuous function $\sigma(t)$ satisfies

$$\int_0^{+\infty} \sigma(t)\mathrm{d}t \leq \bar{\sigma} \tag{7}$$

where $s \in \mathscr{R}^n$, $\sigma(t) > 0$ and $\bar{\sigma} > 0$. The following inequality can be get

$$|s| \leq \frac{s^2}{\sqrt{s^2+\sigma^2(t)}} + \sigma(t) \tag{8}$$

Lemma 4 [19]: In view of the command filter, it is designed as

$$\begin{cases} \dot{\rho}_1 = \omega\rho_2 \\ \dot{\rho}_2 = -2\chi\omega\rho_2 - \omega(\rho_1 - \alpha_1) \end{cases} \tag{9}$$

where ρ_1 and ρ_2 are the command filter state variables. The initial value of ρ_1 is the same as $\alpha_1(0)$, and $\rho_2 = 0$. α_1 is the input variable, it satisfies $|\dot{\alpha}_1| \leq l_1$, $|\ddot{\alpha}_1| \leq l_2$ for all $t \geq 0$, l_1 and l_2 are positive constants. Then for any $\mu > 0$, there exist $\omega > 0$ and $0 < \chi \leq 1$, such that $|\rho_1 - \alpha_1| \leq \mu$, $|\dot{\rho}_1|$, $|\ddot{\rho}_1|$ are bound.

Remark 1: In the subsequent backstepping design, Lemma 4 will be employed to obtain the derivative of the virtual control law α_1 while generating a compensated tracking error signal z_{ec}, thereby eliminating the differential explosion problem inherent in conventional backstepping.

3. Control design

In this section, to achieve compensation for actuator with input saturation, a stable auxiliary system is introduced at first. Then, the event-triggered adaptive asymptotic tracking control is designed.

3.1. Auxiliary system design

Considering the influence of vibration problems on the suspension system under the condition of zero dynamics, a linear filter $\bar{x}_3 = x_3\varsigma/(s+\varsigma)$ is introduced into the controller design. So, the equations of the quarter-car ASS (Equation (3)) can be modified as

$$\begin{cases} \dot{x}_1 = x_2 \\ \dot{x}_2 = h(x) + \kappa u_m \\ \dot{\bar{x}}_3 = \varsigma(x_3 - \bar{x}_3) \\ \dot{x}_3 = x_4 \\ \dot{x}_4 = \dfrac{1}{m_u}(f_t + f_v - f_w - f_r - u_m) \end{cases} \tag{10}$$

where $\varsigma > 0$ is the parameter of the low-pass filter.

In view of the problem of the actuator input saturation, an auxiliary system is introduced [24].

$$\begin{cases} \dot{\lambda}_1 = -a_1\lambda_1 + \lambda_2 \\ \dot{\lambda}_2 = -a_2\lambda_2 + \delta b \end{cases} \tag{11}$$

where λ_1 and λ_2 are the state variables, and the initial values are zeros for λ_1 and λ_2.

The auxiliary system in the above equation can also be written as

$$\begin{bmatrix} \dot{\lambda}_1 \\ \dot{\lambda}_2 \end{bmatrix} = \begin{bmatrix} -a_1 & 1 \\ 0 & -a_2 \end{bmatrix} \begin{bmatrix} \lambda_1 \\ \lambda_2 \end{bmatrix} + \begin{bmatrix} 0 \\ b \end{bmatrix} \delta \tag{12}$$

where $a_1 > 0$ and $a_2 > 0$ are design parameters, $\delta = u_m - u$. Let $A_a = \begin{bmatrix} -a_1 & 1 \\ 0 & -a_2 \end{bmatrix}$, according to the Hurwitz criterion, A_a is Hurwitz matrix. When $t \to \infty$, $\lambda_i \to 0$, $i = 1, 2$. And it can be known from Hurwitz criterions, the auxiliary system in Equation (11) is stable.

3.2. *Event-triggered adaptive neural asymptotic tracking controller design*

According to the constructed auxiliary system (Equation (11)) and using the adaptive backstepping control theory, the design of event-triggered adaptive neural asymptotic tracking control is as follows.

Define the track error z_e as

$$z_e = x_1 - \bar{x}_3 - \lambda_1 \tag{13}$$

Differentiating z_e, it renders

$$\begin{aligned} \dot{z}_e &= \dot{x}_1 - \dot{\bar{x}}_3 - \dot{\lambda}_1 \\ &= x_2 - \varsigma(x_3 - \bar{x}_3) - (-a_1\lambda_1 + \lambda_2) \end{aligned} \tag{14}$$

In order to exclude error of command filter, define the compensated signal z_{ec} as

$$z_{ec} = z_e - \eta_1 \tag{15}$$

with variable η_1 satisfies

$$\dot{\eta}_1 = -k_z\eta_1 + \rho_1 - \alpha_1 \tag{16}$$

where the initial value of η_1 is zero, ρ_1 is the command filter output. Differentiating z_{ec}, it renders

$$\dot{z}_{ec} = x_2 - \varsigma(x_3 - \bar{x}_3) + a_1\lambda_1 - \lambda_2 + k_z\eta_1 - \rho_1 + \alpha_1 \tag{17}$$

Define the track error r_e as

$$r_e = x_2 - \rho_1 - \lambda_2 \tag{18}$$

By substituting Equation (18) to Equation (17), it renders

$$\dot{z}_{ec} = r_e - \varsigma(x_3 - \bar{x}_3) + a_1\lambda_1 + k_z\eta_1 + \alpha_1 \tag{19}$$

Design the virtual control α_1 as

$$\alpha_1 = -k_z z_e + \varsigma(x_3 - \bar{x}_3) - a_1\lambda_1 \tag{20}$$

By substituting Equation (20) to Equation (19), $\dot{z}_{ec}$ can be rewritten as

$$\dot{z}_{ec} = r_e + k_z\eta_1 - k_z z_e \tag{21}$$

Select the Lyapunov function as $V_z = z_{ec}^2/2$. From Equation (15), the time derivative of V_z is

$$\begin{aligned} \dot{V}_z &= z_{ec}(r_e + k_z\eta_1 - k_z z_e) \\ &= z_{ec}r_e - k_z z_{ec}^2 \end{aligned} \tag{22}$$

Differentiating r_e, it renders

$$\begin{aligned} \dot{r}_e &= \dot{x}_2 - \dot{\rho}_1 - \dot{\lambda}_2 \\ &= h(x) + \kappa u_m - \dot{\rho}_1 - (-a_2\lambda_2 + \delta b) \end{aligned} \tag{23}$$

Let $b = \kappa$, then substituting $\delta = u_m - u$ to Equation (23), $\dot{r}_e$ can be rewritten as

$$\dot{r}_e = h(x) + \kappa u - \dot{\rho}_1 + a_2\lambda_2 \tag{24}$$

From Lemma 1, it has

$$\kappa^{-1}h(x) + z_{ec} = W^{\mathrm{T}}\varphi(s_r) + \varepsilon(s_r) \tag{25}$$

where $s_r = [z_{ec}, z_s, z_u, \dot{z}_s, \dot{z}_u]^{\mathrm{T}}$. Choose the Lyapunov function as $V_r = r_e^2/2\kappa$. From Equation (25), the time derivative of V_r is

$$\begin{aligned}\dot{V}_r =& r_e\left(h(x) + \kappa u - \dot{\rho}_1 + a_2\lambda_2\right)\kappa^{-1} \\ =& W^{\mathrm{T}}\varphi r_e + \varepsilon r_e + r_e\left(-\dot{\rho}_1 + a_2\lambda_2\right)\kappa^{-1} + r_e u - z_{ec}r_e\end{aligned} \tag{26}$$

Design the ETC of u as

$$u(t) = \omega\left(t_j\right), t \in \left(t_j, t_{j+1}\right] \tag{27}$$

where t_j is the last triggering instant, and $j = 0, 1, 2, \cdots, +\infty$. $\omega(t)$ is the command control law of $u(t)$. By defining the error as $e(t) = \omega(t) - u(t)$, the trigger condition can be structured as

$$t_{j+1} = \{t > t_j \wedge |e| \geq a_r|u(t)| + b_r\} \tag{28}$$

where $b_r > 0$ and $0 < a_r < 1$ are the adjusting parameters. According to study [38], Equations (27) and (28), we are able to denote $\omega(t)$ as $\omega(t) = (1+\delta_1 a_r)u(t) + \delta_2 b_r$. So, $u(t)$ can be expressed as

$$u(t) = \frac{\omega(t)}{(1+\delta_1 a_r)} - \frac{\delta_2 b_r}{(1+\delta_1 a_r)} \tag{29}$$

where $\delta_1 \in (-1, 1)$, $\delta_2 \in (-1, 1)$. By substituting Equation (29) to Equation (26), $\dot{V}_r$ can be written as

$$\begin{aligned}\dot{V}_r =& \frac{r_e\omega(t)}{(1+\delta_1 a_r)} - \frac{r_e\delta_2 b_r}{(1+\delta_1 a_r)} \\ &+ W^{\mathrm{T}}\varphi r_e + r_e\left(-\dot{\rho}_1 + a_2\lambda_2\right)\kappa^{-1} \\ &+ \varepsilon r_e - z_{ec}r_e\end{aligned} \tag{30}$$

According to Lemma 2, the following inequality holds

$$W^{\mathrm{T}}\varphi r_e + \varepsilon r_e - \frac{r_e\delta_2 b_r}{1+\delta_1 a_r} \leq \beta_r\psi|r_e| \tag{31}$$

where $\beta_r = \max\left\{b_r/(1-a_r) + \bar{\varepsilon}, \|W\|\right\}$, and $\psi = \|\varphi\| + 1$. It can be observed that the influence of $\bar{\varepsilon}_r$ and $\|W\|$ are all covered by one parameter β_r. Thus, it constructs a single-parameter adaptive law, which captures the core concept of the MLP technique. From Equation (8), the inequality of Equation (31) can be rewritten as

$$\beta_r\psi|r_e| \leq \frac{\beta_r\psi^2 r_e^2}{\sqrt{\psi^2 r_e^2 + \sigma^2}} + \beta_r\sigma \tag{32}$$

By substituting Equation (32) to Equation (30), $\dot{V}_r$ can be expressed as

$$\begin{aligned}\dot{V}_r \leq& \frac{r_e\omega(t)}{1+\delta_1 a_r} + \frac{\beta_r\psi^2 r_e^2}{\sqrt{\psi^2 r_e^2 + \sigma^2}} + \beta_r\sigma - z_{ec}r_e \\ &+ r_e\left(-\dot{\rho}_1 + a_2\lambda_2\right)\kappa^{-1}\end{aligned} \tag{33}$$

Design $\omega(t)$ as

$$\begin{aligned}\omega(t) = &-(1+a_r)(k_e r_e + \frac{\hat{\beta}_r \psi^2 r_e}{\sqrt{\psi^2 r_e^2 + \sigma^2}} \\ &- \dot{\rho}_1 \kappa^{-1} + a_2 \lambda_2 \kappa^{-1})\end{aligned} \tag{34}$$

where the estimate of β_r is $\hat{\beta}_r$. k_e is a positive constant. Define the $\tilde{\beta}_r = \beta_r - \hat{\beta}_r$. By inserting Equation (34) into Equation (33), it renders

$$\dot{V}_r \leq -k_e r_e^2 + \frac{\tilde{\beta}_r \psi^2 r_e^2}{\sqrt{\psi^2 r_e^2 + \sigma^2}} + \beta_r \sigma - z_{ec} r_e \tag{35}$$

The $\hat{\beta}_r$ is intended to eradicate the term of $\tilde{\beta}_r$ in Equation (35), then it can be designed as

$$\dot{\hat{\beta}}_r = \frac{\lambda_r \psi^2 r_e^2}{\sqrt{\psi^2 r_e^2 - \sigma^2}} + \lambda_r \hat{\beta}_r \sigma \tag{36}$$

where $\lambda_r > 0$. Consider the Lyapunov function $V_\beta = \tilde{\beta}_r^2 \big/ 2\lambda_r$. Note that $\dot{\tilde{\beta}}_r = -\dot{\hat{\beta}}_r$, and according to using Young's inequality, $\hat{\beta}_r \tilde{\beta}_r \leq \beta_r^2 / 4$. Differentiating V_β along with Equation (36), it yields

$$\dot{V}_\beta \leq -\frac{\tilde{\beta}_r \psi^2 r_e^2}{\sqrt{\psi^2 r_e^2 + \sigma^2}} + \frac{\beta_r^2}{4} \sigma \tag{37}$$

The pseudo codes in Algorithm 1 illustrate how the ETC scheme can be implemented in practice. Notably, the proposed scheme is computationally simple, making it suitable for deployment on current microcomputers.

Algorithm 1 ETC adaptive neural asymptotic tracking control

1. Initialize x, y, z, θ, ψ, ϕ, $\hat{\beta}_r$
2. **for** computing time from $i = 1$ to $i = N$ **do**
3. calculate $\omega(t)$ from Equation (34)
4. **if** triggering condition (Equation (28)) is satisfied **then**
5. assign $t_j = t_0 + it_s$, renew $u(t)$ from Equation (27)
6. **end if**
7. update $\hat{\beta}_r$ using Equation (36)
8. execute control law $u(t)$ in quarter-car ASS of Equation (3)
9. **end for**

4. Stability and constraint analysis

In this section, the stability of the closed-loop system is scrupulously proven. In addition, the zero dynamics and constraint conditions are also theoretically analyzed.

4.1. Stability analysis

The proposed scheme can be synthesized into the following theorem.

Theorem 1: For the ASS described by Equations (3) and (10), all the states are assumed to be defined in a compact set. the event-triggered adaptive neural asymptotic tracking control consisting of adaptive

law (Equation (36)), triggering condition (Equation (28)), and the control law (Equation (33)), can ensure the tracking errors of z_e and r_e are asymptotic convergence.

Proof: The Lyapunov candidate can be chosen as $V = V_z + V_r + V_\beta$. Differentiating V, and synthesizing Equations (28), (33), (36), it yields

$$\dot{V} \leq -k_z z_{ec}^2 - k_e r_e^2 + \beta_r \sigma + \frac{\beta_r^2}{4}\sigma \tag{38}$$

According to Lemma 3, we can get that $\int_0^t \left(\beta_r + \beta_r^2/4\right)\sigma dt \leq \left(\beta_r + \beta_r^2/4\right)\bar{\sigma}$. So integrating both sides of Equation (38), it can be written as

$$V(t) - V(0) \leq -\int_0^t \left(k_z z_{ec}^2 + k_e r_e^2\right) \mathrm{d}t + \left(\beta_r + \frac{\beta_r^2}{4}\right)\bar{\sigma} \tag{39}$$

From Equation (39), it can be deduced that $V(t) - V(0)$ is bounded. By exchanging the terms on both sides of the inequality, Equation (39) is formulated as

$$\int_0^t \left(k_z z_{ec}^2 + k_e r_e^2\right) \mathrm{d}t \leq V(0) - V(t) + \left(\beta_r + \frac{\beta_r^2}{4}\right)\bar{\sigma} \tag{40}$$

Given that the right side of the inequality is bounded, it is known from Barbalat's lemma that $z_{ec} \to 0$ and $r_e \to 0$ while $t \to +\infty$. The proof is completed.

4.2. Analysis of zero dynamics and constraint conditions

Proof the stability of zero dynamics: As can be seen from the above section, it can be seen that the proposed control scheme is based on subsystem of Equation (10), that is

$$\begin{cases} \dot{x}_1 = x_2 \\ \dot{x}_2 = h(x) + \kappa u_m \\ \dot{\bar{x}}_3 = \varsigma(x_3 - \bar{x}_3) \end{cases} \tag{41}$$

As the subsystem (Equation (41)) is the order of 3, while the order of Equation (10) is 5, there has a zero dynamics in Equation (10). Therefore, the zero dynamics consist of another state variables. Let $y = x_1 - \bar{x}_3 = 0$, we have

$$\ddot{y} = \frac{1}{m_b}\left(-f_v - f_t + u_m\right) - \varsigma\left[x_4 - \varsigma\left(x_3 - \bar{x}_3\right)\right] \tag{42}$$

By substituting Equation (42) to Equation (10), the zero dynamics system is

$$\begin{cases} \dot{\bar{x}}_3 = \varsigma(x_3 - \bar{x}_3) \\ \dot{x}_3 = x_4 \\ \dot{x}_4 = \dfrac{1}{m_u}\left\{-m_b\varsigma\left[x_4 - \varsigma(x_3 - \bar{x}_3)\right] - k_t x_3 - c_t x_4 + C\right\} \end{cases} \tag{43}$$

where $C = k_t z_r + c_t \dot{z}_r$.

From Assumption 1, one has $|C| \leq \bar{C}$. $\bar{C}$ is a positive constant. Equation (43) can be rewritten as:

$$\dot{x} = Ax + BC \tag{44}$$

where $x = \begin{bmatrix} \bar{x}_3 \\ x_3 \\ x_4 \end{bmatrix}$, $A = \begin{bmatrix} -\varsigma & \varsigma & 0 \\ 0 & 0 & 1 \\ A_1 & A_2 & A_3 \end{bmatrix}$, $B = \begin{bmatrix} 0 \\ 0 \\ 1 \end{bmatrix}$, $A_1 = -\dfrac{m_s\varsigma^2}{m_u}$, $A_2 = \dfrac{m_s\varsigma^2 - k_t}{m_u}$, $A_3 = \dfrac{c_t - m_s\varsigma}{m_u}$.

The Lyapunov function is selected as $V_D = x^{\mathrm{T}}Px$. $\dot{V}_D$ is obtained from the following equation,

$$\dot{V}_D = \dot{x}^{\mathrm{T}}Px + x^{\mathrm{T}}P\dot{x} \tag{45}$$

Since A is a Hurwitz matrix, meaning that the eigenvalues of A have negative real parts, for a given positive-definite matrix Q, there must exist a positive-definite matrix P to satisfy $A^{\mathrm{T}}P + PA = -Q$. Then, $\dot{V}_D$ can be rewritten as

$$\dot{V}_D = -x^{\mathrm{T}}Qx + 2x^{\mathrm{T}}PBC \tag{46}$$

By using Young's inequality, $2x^{\mathrm{T}}PBC \leq \dfrac{x^{\mathrm{T}}PBB^{\mathrm{T}}Px}{\tau_1} + \tau_1 C^{\mathrm{T}}C$. Equation (47) can be written as

$$\dot{V}_D \leq -x^{\mathrm{T}}Qx + \frac{1}{\tau_1}x^{\mathrm{T}}PBB^{\mathrm{T}}Px + \tau_1 C^{\mathrm{T}}C \tag{47}$$

where τ_1 is positive constant to be designed. Then, Equation (48) becomes

$$\dot{V}_D \leq \lambda V_D + \nabla \tag{48}$$

where $\lambda = \lambda_{\min}\left(P^{-\frac{1}{2}}QP^{-\frac{1}{2}}\right) - \dfrac{1}{\tau_1}\lambda_{\max}\left(P^{\frac{1}{2}}BB^{\mathrm{T}}P^{\frac{1}{2}}\right)$, $\nabla = \tau_1\bar{C}^2$, with $C^{\mathrm{T}}C \leq \bar{C}^2$. Based on the above analysis, we can get that $\bar{x}_3$, x_3 and x_4 are bounded as $t \to \infty$.

Proof of constraint conditions: For the ride comfort, the body acceleration $\ddot{z}_s$ is closely related to it. By obtaining Equation (4), it can easily get

$$\ddot{z}_s = h(x) + \kappa u_m \tag{49}$$

where the function $h(x)$ is bounded and κ is also the bounded parameter. According to Equation (2), $|u_m| \leq \bar{u}_m$. Therefore, it is known that $\ddot{z}_s$ is bounded, which implies stable ride comfort.

For the ride safety, we will prove that $|f_w + f_r| \leq (m_s + m_u)\,g$ is satisfied. Since

$$\begin{aligned} |f_w + f_r| &= |k_t(x_3 - z_r) + c_t(x_4 - \dot{z}_r)| \\ &= |k_t x_3 + c_t x_4 + C| \end{aligned} \tag{50}$$

According to Equations (43) and (49), x_3, x_4 and C are bounded. If the initial values and design parameters are appropriately adjusted to achieve $(k_t x_3 + c_t x_4 + C) \leq (m_s + m_u)\,g$, ride safety will be ensured.

Based on the above analysis, we will demonstrate the suspension working space limit $|x_1 - x_3| \leq \bar{z}_{max}$ is to be satisfied. According to the Equations (13) and (15), we can easily get $x_1 = z_{ec} + \eta_1 + \bar{x}_3 + \lambda_1$. Then, the maximum of the body vertical displacement is $|x_1 - x_3| \leq |z_{ec}| + |\eta_1| + |\bar{x}_3| + |\lambda_1| + |x_3|$. From Theorem 1, Equations (12) and (49), we know that z_{ec}, η_1, $\bar{x}_3$, λ_1 and x_3 are bounded. Consequently, we can derive $|x_1 - x_3| \leq z_{max}$. If we tune the parameters and initial values appropriately to hold $z_{max} \leq \bar{z}_{max}$, the suspension working space limit is ensured.

Remark 2: To verify the non-Zeno behavior, we analyze the inter-execution time $\{t_{j+1}-t_j\}$. From the triggering condition (Equation (28)) and the boundedness of $u(t)$, there exists a minimum positive inter-event time $T_{\min}>0$ such that $t_{j+1}-t_j \geq T_{\min}$ for all j, which excludes the Zeno phenomenon.

5. Simulation and experiments

In this section, to verify the effectiveness of the control method proposed for the two-degree-of-freedom vehicle suspension model, we will conduct comparative experiments on without input saturation scheme.

Considering the uncertainty and complexity of vehicle driving scenarios, simulation experiments were designed on "bump road", "random road", and "step road", respectively. The result analysis shows that the designed control algorithm has significant advantages in the stability of vehicle active suspension. The parameters and data a quarter-car ASS are chosen as Table 1.

Table 1. The parameters and data of a quarter-car ASS.

Parameter	Data	Parameter	Data
m_b	900 kg	m_u	100 kg
k_t	20,000 N/m	k_a	10,000 N/m
c_a	2600 N·s/m	c_t	1000 N·s/m
c_b	600 N·s/m	c_c	500 N·s/m
$\bar{u}_m$	500 N	ς	0.1
γ	10	$\bar{z}_{max}$	0.15

To minimize the Lyapunov function and ensure that the system's state trajectory follows the desired reference while maintaining stability under input saturation, we determined the parameter values through a combination of empirical analysis and exhaustive search with a step size of 0.1. Optimize the tuning parameters with a step size of 0.1 by minimizing the target performance indicators $\int_2^{10} x_1 dt$ to obtain the ideal parameters for optimal control performance. The specific values are provided below. A RBF NN with 11 neurons is used in this case. The command filter parameters $\chi=0.5$ and $\omega=10$. The parameters $a_1=1$ and $a_2=2$ in auxiliary dynamic system. The else control parameters are selected as $k_z=1$, $a_r=0.3$, $b_r=0.02$ and $\lambda_r=5$. The integral-bounded function is chosen as $\sigma=0.02\ \exp(-0.02t)$. The simulation duration is set to 10 seconds.

So as to demonstrate the excellence of the proposed scheme, we compared three control methods separately, namely conventional passive suspension, the proposed scheme without input saturation and fuzzy logic system (FLS) observer scheme in study, which are marked as "Passive suspension", "Without input saturation scheme" and "FLS observer scheme". The control law for the proposed scheme without input saturation is designed as

$$u=-(1+a_r)(k_e r_e+\frac{\hat{\beta}_r \psi^2 r_e}{\sqrt{\psi^2 r_e^2+\sigma^2}}-\dot{\rho}_1 \kappa^{-1}) \tag{51}$$

where the control parameters remain the same as above. It is assumed that the initial value is set as $z_s=0.15$, and other initial values are zeros. The results of the simulation are presented as follows.

5.1. Simulation results

To evaluate the effectiveness of the proposed control scheme, comprehensive simulations are conducted under three typical road excitations: bump road, random road, and step road.

5.1.1. Bump road

To prove the effectiveness of the proposed scheme, we first design sudden disturbance to simulate real bump road. Substituting Equation (44) into Equation (45) results in

$$\dot{V}_D = x^{\mathrm{T}}\left(A^{\mathrm{T}}P + PA\right)x + 2x^{\mathrm{T}}PBC \tag{52}$$

$$z_r = \begin{cases} \dfrac{h}{2}(1-\cos(\dfrac{2\pi}{n}vt)),\ 4 \le t \le 6 \\ 0,\ \text{otherwise} \end{cases}$$

where $h = 0.05$ m is the bump height, $n = 200/3$ m is the bump width and $v = 20$ m/s is the vehicle velocity. The bump road is shown in Figure 2a.

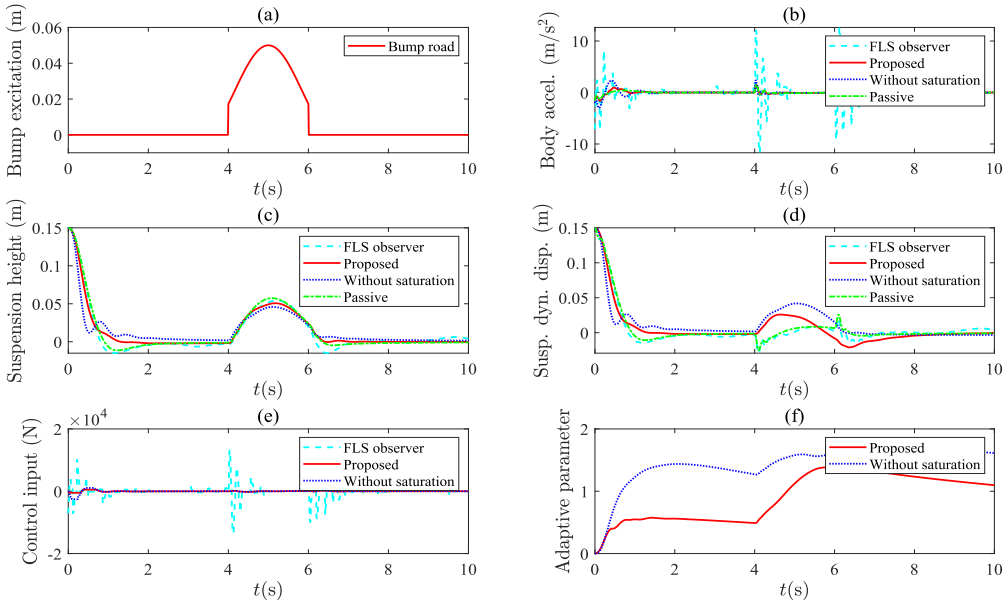

Figure 2. Characteristics of the proposed scheme under bump road: **(a)** Bump road; **(b)** Vehicle body acceleration; **(c)** Suspension height; **(d)** Suspension dynamic displacement; **(e)** Control inputs; **(f)** Adaptive parameters.

Figure 2b shows the vehicle body acceleration at the center of gravity under different control strategies. It is evident that the proposed scheme achieves a faster convergence speed and smaller acceleration amplitude compared to the "without input saturation" scheme when dealing with uneven road surfaces. Figure 2c compares the suspension height development. The suspension working space, which reflects vehicle shake during driving, changes dramatically under passive suspension and the "FLS observer scheme", while the proposed method (even without input saturation) exhibits much smaller fluctuations, highlighting its superiority. Figure 2d presents the suspension dynamic displacement under bump road disturbance. The proposed scheme recovers to stability faster at $t = 1$ s; although its recovery speed is slightly slower after passing the bump, the peak displacement is smaller. Compared with the other three schemes, the

active suspension provides better stability of body vertical displacement than passive suspension, and the proposed method outperforms both the "without input saturation" and the "FLS observer" schemes. Figure 2e compares the control inputs. The proposed control strategy effectively satisfies input saturation constraints. Moreover, compared with the "FLS observer scheme", it requires smaller control inputs, thereby significantly saving control resources. Figure 2f shows the evolution of the adaptive parameter $\hat{\beta}_r$ in the proposed method; it tends to a stable constant and remains bounded eventually.

5.1.2. Random road

Due to random road uncertain fluctuation characteristics, these stochastic variations manifest as irregular vertical displacements and roughness profiles that cannot be precisely predicted using deterministic models. By incorporating such random road inputs into the analysis, the simulation framework aligns more closely with the complex outdoor road conditions encountered in real-world scenarios. So it is closer to the actual ground information of complex outdoor roads. Consequently, the dynamic responses of the suspension system under these stochastic disturbances more accurately reflect its actual working conditions.

Figure 3a shows the random road profile. Figure 3b presents the vehicle body acceleration under random road changes. Compared to the "FLS observer scheme", the proposed method achieves lower vehicle acceleration, and both schemes can reach fixed stability in a short time. Figure 3c illustrates the active suspension height. It can be seen that the suspension height also achieves fixed stability quickly under random road variations. Figure 3d shows the suspension dynamic displacement, which similarly reaches fixed stability in a short time. Figure 3e compares the control inputs under different control schemes. The proposed scheme achieves smaller control inputs and effectively satisfies input saturation constraints. Figure 3f shows the adaptive parameter of the proposed scheme; it can reach a fixed stable value at 2 seconds.

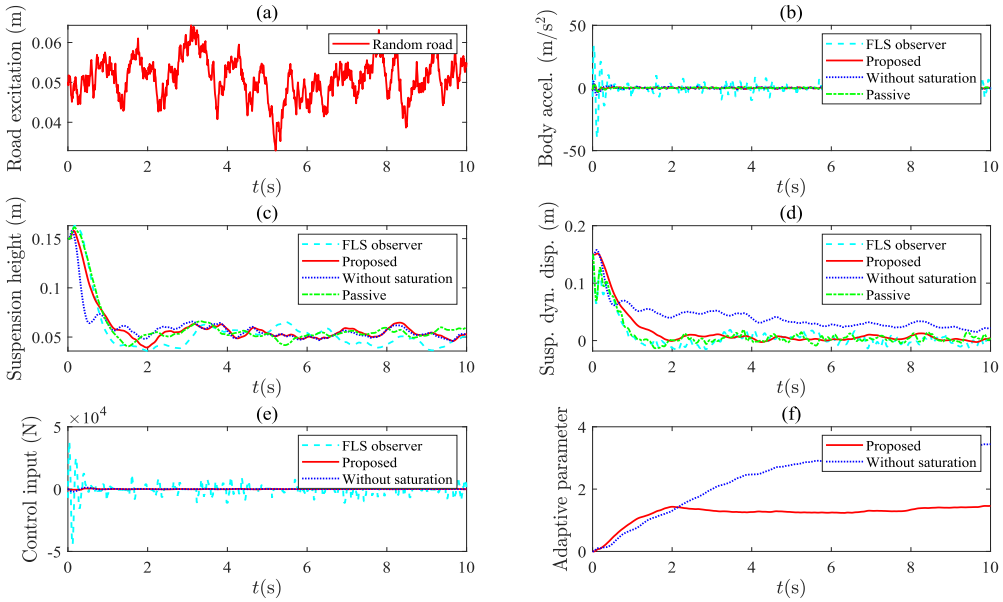

Figure 3. Characteristics of the proposed scheme under random road: **(a)** Random road; **(b)** Vehicle body acceleration; **(c)** Suspension height; **(d)** Suspension dynamic displacement; **(e)** Control inputs; **(f)** Adaptive parameters.

5.1.3. Step road

The control effect of the proposed scheme can be simulated by the step road in scenarios where the front and rear displacement of the vehicle exhibit inconsistency. Figure 4 illustrates the operational characteristics of active suspension while driving on the step road.

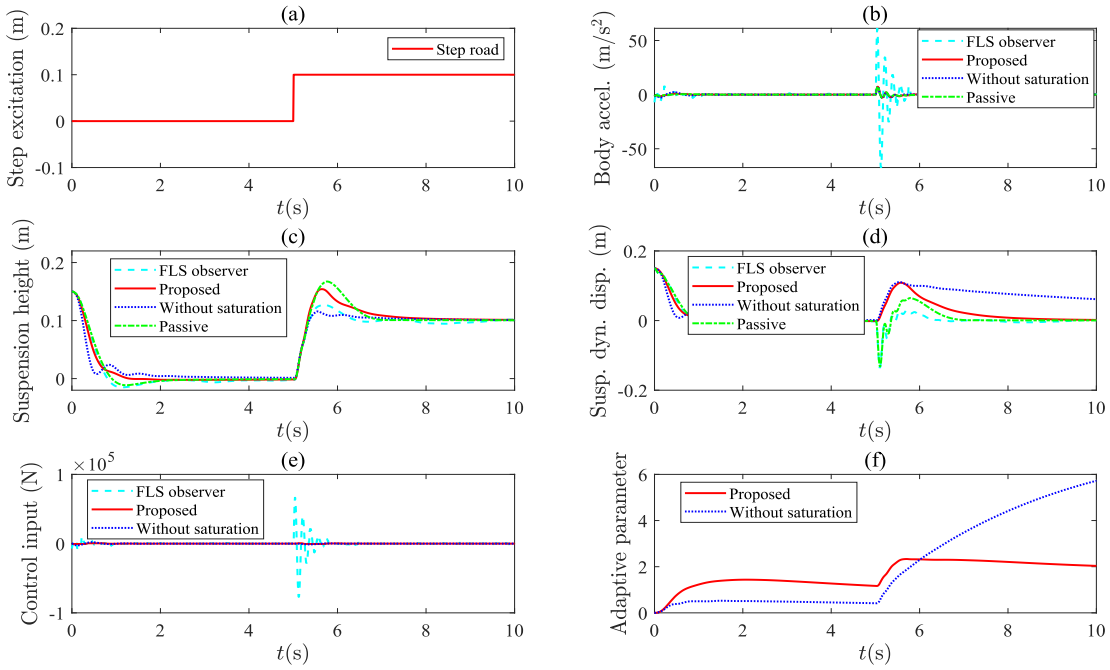

Figure 4. Characteristics of the proposed scheme under step road: **(a)** Step road; **(b)** Vehicle body acceleration; **(c)** Suspension height; **(d)** Suspension dynamic displacement; **(e)** Control inputs; **(f)** Adaptive parameters.

Figure 4b presents the vehicle body acceleration. It can be seen that when encountering step signals, the influence on body acceleration is also smaller under the proposed scheme. Figure 4c shows the evolution of suspension height. The suspension of the designed strategy can reach stability faster in the early stage. Compared to the other three methods, the proposed strategy has smaller suspension height changes when passing over the step road surface. Figure 4d illustrates the suspension dynamic displacement. In the presence of a step signal, the proposed strategy stabilizes rapidly relative to the "without input saturation scheme". However, passive suspension and the "FLS observer scheme" exhibit smaller suspension dynamic displacements, which may be because the "FLS observer scheme" consumes more control energy to achieve that effect. In addition, when passing over the road, the "FLS observer scheme" strategy generates violent and rapid fluctuations, which is unfavorable. Notably, in scenarios where one wheel encounters an elevated position while the other remains on a level road surface, the corresponding suspension actively compresses. This control characteristic plays a crucial role in facilitating vehicle operation within outdoor environments. Figure 4e compares the control inputs. Based on observations from Figure 4e and Figure 4f, it is evident that the proposed control scheme can achieve smaller control inputs compared with other schemes. Figure 4f shows the adaptive parameters. It is evident that the adaptive parameters achieve stability more rapidly following the occurrence of a step signal.

Figure 5 illustrates the change of the inter-event time in the controller-to-actuator channel in "bump road", "random road", and "step road". Benefiting from the design of ETC, the proposed scheme has a total of 181, 374, and 145 triggering instants, of which the maximum inter-event time of 0.67 s, 0.27 s, 0.67 s, and the minimum of 0.01 s, respectively. In contrast, the proposed scheme without input saturation has a total of 1001 samples with a signal sampling period of 0.01 s. Therefore, the ETC employed in this paper can significantly reduce communication resources.

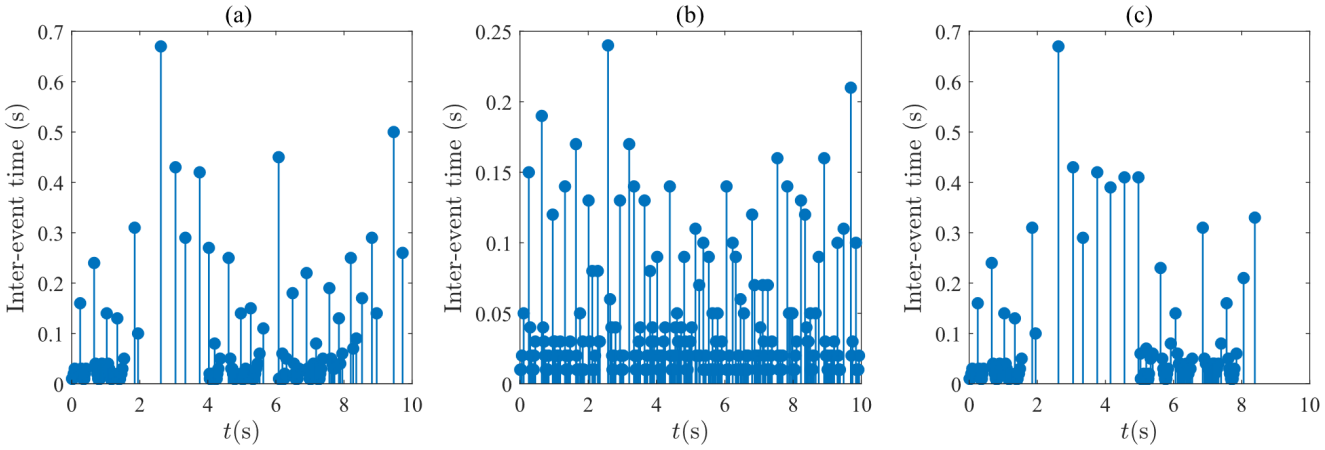

Figure 5. Inter-event time of the proposed scheme under different roads: **(a)** Bump road; **(b)** Random road; **(c)** Step road.

To further demonstrate the superiority of the proposed approach, we performed a quantitative index analysis of simulation results from the four control methods, as shown in Table 2. Specifically, we conduct four quantitative comparative analyses on "Bump road", "Random road" and 'Step road'. The analysis indexes are "Suspension dynamic displacement (SDD)", "Suspension height (SH)", "Vehicle body acceleration (VBA)", and "control energy". In each index, we separately analyzed the root mean square error (RMSE), maximum overshoot, settling time, and control energy consumption of each control method on different road surfaces. According to the analysis in Table 2, the proposed control strategy may have slightly inferior performance on certain road surfaces compared to the other three methods. However, overall, the proposed method has better performance. Especially in terms of controlling input energy consumption and control accuracy, it displays the best results and has a better anti-saturation effect.

Table 2. Quantitative indexes analysis of four control methods.

Indexes	Sub-index	FLS observer			Without saturation			Passive			Proposed		
		Bump	Random	Step	Bump	Random	Step	Bump	Random	Step	Bump	Random	Step
SDD	RMSE (m)	0.0326	0.0499	0.0778	**0.0235**	0.0469	**0.0306**	0.0322	0.0474	0.0733	0.0286	**0.0253**	0.0616
	Max (m)	0.0293	0.0182	0.1362	0.0419	0.0549	0.1105	**0.0252**	0.0189	0.1316	0.0259	**0.0125**	**0.1087**
	Time (s)	2.43	3.25	2.35	2.25	6.27	3.15	2.63	3.13	2.35	**1.27**	**1.98**	**1.32**
SH	RMSE (m)	0.0281	0.0265	0.0307	0.0265	**0.0192**	0.0315	**0.0236**	0.0257	0.0344	0.0283	0.0233	**0.0265**
	Max (m)	0.0543	0.0652	0.1276	**0.0458**	0.0657	0.1541	0.0573	0.0660	0.1673	0.0507	**0.0646**	**0.1157**
	Time (s)	2.31	3.98	2.04	3.05	2.62	3.03	2.20	2.23	2.04	**1.30**	**1.84**	**1.52**
VBA	RMSE (m/s²)	1.9424	5.0681	6.8430	0.2823	0.7095	0.7647	0.5125	0.4431	**0.6371**	**0.2350**	**0.4309**	0.6681
	Max (m/s²)	12.6438	10.1563	67.3657	2.4245	2.0033	**7.3057**	1.4608	1.1027	7.3290	**1.4584**	**0.8279**	7.3276
	Time (s)	2.15	1.28	1.51	0.94	0.96	0.99	0.90	0.83	0.99	**0.89**	**0.58**	**0.81**
Energy (N)		894,554.6	3,258,927.1	1,853,233.8	125,505.3	135,226.6	170,183.9	w/o	w/o	w/o	**66,130.1**	**85,861.1**	**89,144.2**

5.2. *Experimental results*

Based on the simulation results, the proposed strategy not only improves the system's position tracking accuracy but also reduces the control input. The advantage of this strategy lies in its ability to achieve better control performance on any road surface, as long as the system operates within the hardware's capacity.

Figure 6 shows the configuration of the suspension system's experimental platform, which mainly consists of hydraulic components, mechanical parts, and an electronic control module. The detailed technical specifications of the experimental platform are listed in Table 3. The system is equipped with a position sensor and two pressure sensors to ensure accurate experimental measurements. The position sensor is used to detect the system's output displacement, while the pressure sensors monitor the pressure changes in the two chambers on either side of the hydraulic cylinder. During the experiment, to maintain system stability and the accuracy of the results, the supply pressure of the hydraulic system must be kept above 16 MPa. This high-pressure supply ensures stable operation of the hydraulic system under high load and fast dynamic response conditions, which is crucial for accurately evaluating the suspension performance when simulating complex working conditions. Additionally, the electronic control module adjusts the hydraulic system's working state in real-time through a feedback mechanism, further enhancing experimental accuracy and system response speed.

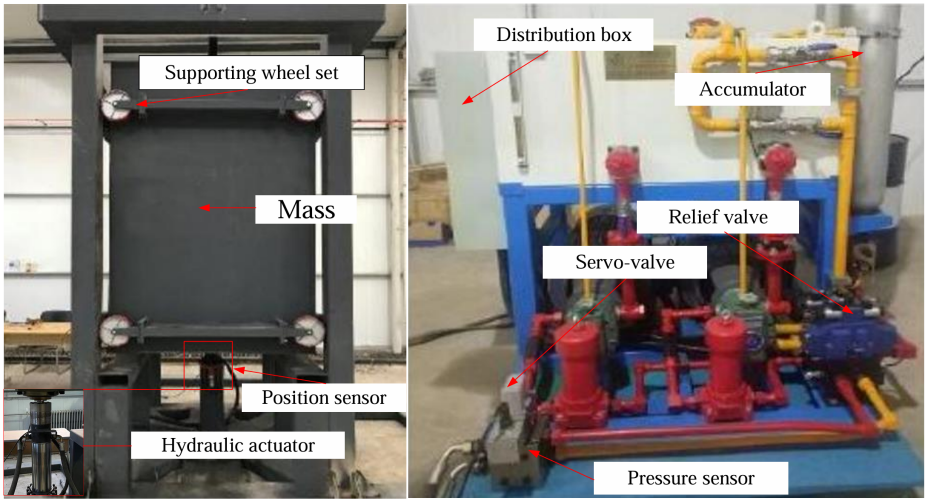

Figure 6. Experimental setup of the suspension system.

Table 3. Specifications of the experiment setup.

Experimental Specifications	**Details**
Hydraulic cylinder piston	Stroke: 0–300 mm SFD234
Servo valve	Command signal: 0 ± 10 mA Bandwidth ≥ 75 Hz
Pressure sensor	Pressure range: 0–40 MPa
Position sensor	Stroke: 0–300 mm
Controller processor	Quad-core 3.1 GHz processor (i5-2400.Intel)
Sampling frequency	1000 Hz
Analog output card	PCI-6208 (16-bit resolution)
Data acquisition card	PCI-1716 (16-bit resolution)

To comprehensively evaluate the performance of the proposed method, we conducted experimental comparisons using both square wave and sine wave signals. Additionally, to validate the superiority of the proposed method, we introduced the "FLS observer scheme" of study and "With input saturation scheme" as baseline comparisons. As shown in Figure 7 and Figure 8, these experiments provide a thorough comparison between the proposed method and other control strategies under different input conditions, allowing for a deeper analysis of the control method's performance across a variety of signal conditions, ensuring a comprehensive and accurate evaluation.

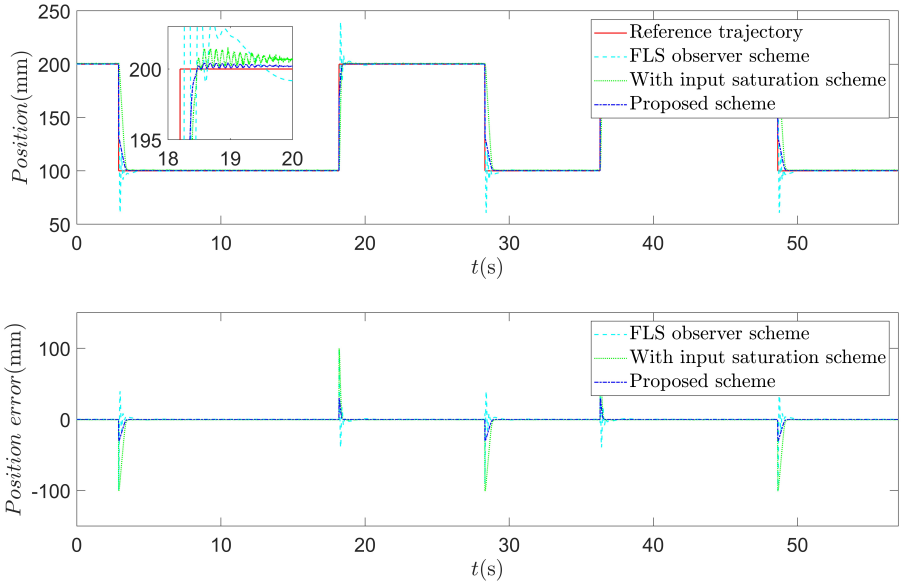

Figure 7. Position tracking performance and error curve of square wave signal.

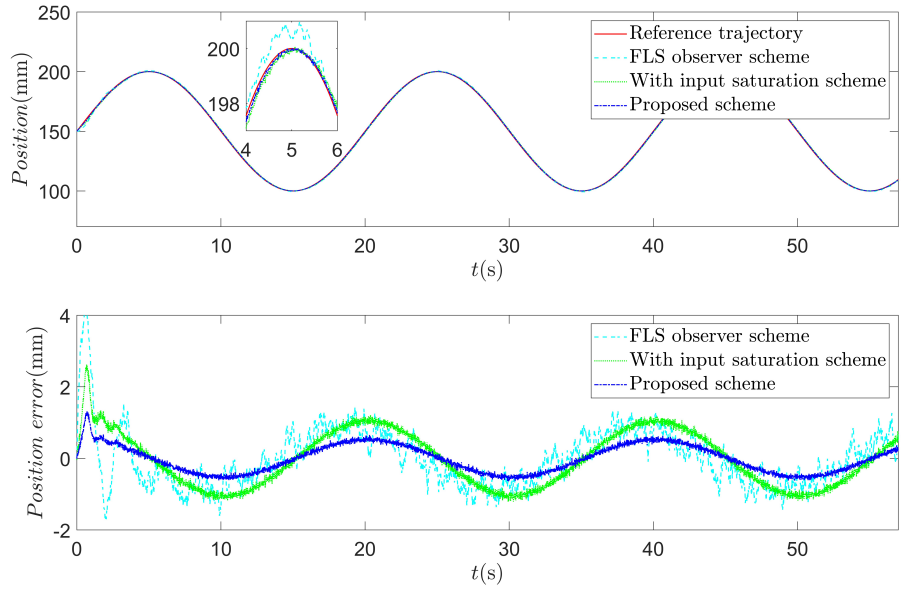

Figure 8. Position tracking performance and error curve of sine wave signal.

In the square wave signal experiment, compared to the "FLS observer scheme", the proposed strategy significantly reduced the steady-state tracking error by 59.82%, while also demonstrating superior convergence speed and accuracy. Specifically, during the system response, the proposed method not

only achieved rapid steady-state convergence but also maintained high precision, effectively minimizing errors caused by input waveform transitions. In the sine wave experiment, the advantages of the proposed method were even more evident. Under this signal condition, the proposed control strategy was able to track the input signal more accurately, further reducing steady-state error and demonstrating superior system stability, where the control precision and robustness outperformed the "FLS observer scheme" and "With input saturation scheme".

Overall, the experimental results clearly demonstrate the superiority of the proposed control strategy across various signal inputs. In particular, the proposed method shows significant improvements in tracking accuracy, steady-state error, and system stability compared to traditional control strategies and baseline methods. These experiments validate the broad applicability and strong advantages of the proposed method in practical applications.

6. Conclusion

This paper has presented an event-triggered adaptive neural asymptotic tracking control scheme for active suspension systems with input saturation, which made use of auxiliary system, command filter method and radial basis function neural network, *etc*. The auxiliary system is constructed to avoid actuator input saturation. Command filter is introduced into the design process to prevent the differential explosion problem. Asymptotic convergence of the tracking error is achieved by fusing integral bounded functions into the control law and adaptive law. The "non-Zeno" behavior is ensured by designing the event-triggered condition with variable threshold. The control performance of the proposed method and the communication saving can be demonstrated in the simulation and experimental. However, while this paper considers the input saturation of the actuator, it ignores the effect of time delay on the control system. In the future, the proposed scheme can be extended to the asymptotic tracking control of active suspension systems for semi-vehicle models and even vehicle models by following the same design concept.

Data availability statement

No supplementary or additional data were generated in this study.

Declaration of generative AI and AI-assisted technologies

The authors did not use generative AI or AI-assisted technologies in the writing of this manuscript.

Acknowledgments

This work is partially supported by the Natural Science Foundation of China (No. U24A6008, No. 52101375), the Hebei Province Natural Science Fund (No. E2024203179), the Science and Technology Project of Hebei Education Department (No. BJ2025114).

Authors' contribution

Conceptualization, Yingjie Deng; validation, Tao Ni; formal analysis, Fangcheng Liu; writing—original draft preparation, Fangcheng Liu, Xiangyu Meng, Yuxin Wu; writing—review and editing, Yingjie Deng, Namkyun Im, Tao Ni, Dingxuan Zhao; supervision, Namkyun Im; funding acquisition, Dingxuan Zhao. All authors have read and agreed to the published version of the manuscript.

Conflicts of interest

Dingxuan Zhao holds the position of Executive Editor for *Advanced Equipment* and has not peer reviewed or made any editorial decisions for this paper. The authors declare no potential conflicts of interest.

References

[1] Theunissen J, Tota A, Gruber P, Dhaens M, Sorniotti A. Preview-based techniques for vehicle suspension control: a state-of-the-art review. *Annu. Rev. Control* 2021, 51:206–235.

[2] Chen G, Jiang Y, Tang Y, Xu X. Revised adaptive active disturbance rejection sliding mode control strategy for vertical stability of active hydro-pneumatic suspension. *ISA Trans.* 2023, 132:490–507.

[3] Sang N, Wei M. Active disturbance rejection control method of active front wheel steering and active suspension system of vehicle. *J. Nanjing Univ. Sci. Technol.* 2017, 41:165–172+185.

[4] Chen C, Gao H, Ding L, Li W, Yu H, *et al.* Trajectory tracking control of WMRs with lateral and longitudinal slippage based on active disturbance rejection control. *Robot. Auton. Syst.* 2018, 107:236–245.

[5] Papadimitrakis M, Alexandridis A. Active vehicle suspension control using road preview model predictive control and radial basis function networks. *Appl. Soft Comput.* 2022, 120(1):108646.

[6] Shao S, Zhou H, Liu H. Distributed model predictive control and implementation for vehicle active suspensions. *IFAC-PapersOnLine* 2018, 51(31):961–966.

[7] Pedro JO, Nhlapo SM, Mpanza LJ. Model predictive control of half-car active suspension systems using particle swarm optimisation. *IFAC-PapersOnLine* 2020, 53(2):14438–14443.

[8] Lin B, Su X, Li X. Fuzzy sliding mode control for active suspension system with proportional differential sliding mode observer. *Asian J. Control* 2019, 21(1):264–276.

[9] Chen H, Liu Y, Liu L, Tong S, Gao Z. Anti-saturation-based adaptive sliding-mode control for active suspension systems with time-varying vertical displacement and speed constraints. *IEEE Trans. Cybern.* 2022, 52(7):6244–6254.

[10] Nguyen DN, Nguyen TA. Proposing an original control algorithm for the active suspension system to improve vehicle vibration: adaptive fuzzy sliding mode proportional-integral-derivative tuned by the fuzzy (AFSPIDF). *Heliyon* 2023, 9(3):e14210.

[11] Pang H, Zhang X, Yang J, Shang Y. Adaptive backstepping-based control design for uncertain nonlinear active suspension system with input delay. *Int. J. Robust Nonlinear Control* 2019, 29(16):5781–5800.

[12] Sun H, Li Y, Xu K, Tong S. Fuzzy adaptive backstepping control for a class of active suspension systems. *IFAC-PapersOnLine* 2018, 51(31):136–141.

[13] Wang Q, Zhao Y, Xu H, Deng Y. Adaptive backstepping control with grey signal predictor for nonlinear active suspension system matching mechanical elastic wheel. *Mech. Syst. Signal Process.* 2019, 131:97–111.

[14] Zhang Y, Liu Y, Wang Z, Bai R, Liu L. Neural networks-based adaptive dynamic surface control for vehicle active suspension systems with time-varying displacement constraints. *Neurocomputing* 2020, 408:176–187.

[15] Liu S, Hao R, Zhao D, Tian Z. Adaptive dynamic surface control for active suspension with electro-hydraulic actuator parameter uncertainty and external disturbance. *IEEE Access* 2020, 8:156645–156653.

[16] Liu Y, Zeng Q, Liu L, Tong S. An adaptive neural network controller for active suspension systems with hydraulic actuator. *IEEE Trans. Syst. Man Cybern.-Syst.* 2020, 50(12):5351–5360.

[17] Homayoun B, Arefi MM, Vafamand N, Yin S. Neural minimal learning backstepping control of stochastic active suspension systems with hydraulic actuator saturation. *J. Franklin Inst.* 2020, 357(18):13687–13706.

[18] Homayoun B, Arefi MM, Vafamand N. Robust adaptive backstepping tracking control of stochastic nonlinear systems with unknown input saturation: a command filter approach. *Int. J. Robust Nonlinear Control* 2020, 30(8):3296–3313.

[19] Ho CM, Tran DT, Nguyen CH, KwanAhn K. Adaptive neural command filtered control for pneumatic active suspension with prescribed performance and input saturation. *IEEE Access* 2021, 9:56855–56868.

[20] Shen Z, Wang Q, Dong S, Yu H. Dynamic surface control for tracking of unmanned surface vessel with prescribed performance and asymmetric time-varying full state constraints. *Ocean Eng.* 2022, 253:111319.

[21] Liu S, Zhang G, Zhang W, Zhang X. Robust fuzzy dynamic surface formation control for underactuated ships using MLP and LFG. *Syst. Sci. Control Eng.* 2022, 10(1):272–281.

[22] Shen Z, Li F, Cao X, Guo C. Prescribed performance dynamic surface control for trajectory tracking of quadrotor UAV with uncertainties and input constraints. *Int. J. Control* 2021, 94(11):2945–2955.

[23] Zhang Y, Chen Z, Sun M. Trajectory tracking control for a quadrotor unmanned aerial vehicle based on dynamic surface active disturbance rejection control. *Trans. Inst. Meas. Control* 2020, 42(12):2198–2205.

[24] Wang T, Li Y. Neural-network adaptive output-feedback saturation control for uncertain active suspension systems. *IEEE Trans. Cybern.* 2022, 52(3):1881–1890.

[25] Zhang M, Jing X, Wang G. Bioinspired nonlinear dynamics-based adaptive neural network control for vehicle suspension systems with uncertain/unknown dynamics and input delay. *IEEE Trans. Ind. Electron.* 2021, 68(12):12646–12656.

[26] Zhang J, Li K, Li Y. Neuro-adaptive optimized control for full active suspension systems with full state constraints. *Neurocomputing* 2021, 458:478–489.

[27] Zhao F, Ge SS, Tu F, Qin Y, Dong M. Adaptive neural network control for active suspension system with actuator saturation. *IET Control Theory Appl.* 2016, 10(14):1696–1705.

[28] Chen M, Ge SS, Ren B. Adaptive tracking control of uncertain MIMO nonlinear systems with input constraints. *Automatica* 2011, 47(3):452–465.

[29] Zhang J, Wang J. Adaptive tracking control of vehicle suspensions with actuator saturations. In *Proceedings of 2015 34th Chinese Control Conference (CCC)*, Hangzhou, China, July 28–30, 2015, pp. 8051–8056.

[30] Zhang Y, Liu Y, Liu L. Minimal learning parameters-based adaptive neural control for vehicle active suspensions with input saturation. *Neurocomputing* 2020, 396:153–161.

[31] Wang G, Chadli M, Chen H, Zhou Z. Event-triggered control for active vehicle suspension systems with network-induced delays. *J. Franklin Inst.* 2019, 356(1):147–172.

[32] Ge X, Ahmad I, Han Q, Wang J, Zhang X. Dynamic event-triggered scheduling and control for vehicle active suspension over controller area network. *Mech. Syst. Signal Process.* 2021, 152:107481.

[33] Deng Y, Liu F, Xu Y, Li F, Ni T, *et al.* Double-channel event-triggered adaptive tracking control of nonstrict-feedback nonlinear systems with separate state transmission. *Adv. Equip.* 2025, 1(1):1–20.

[34] Deng Y, Liu F, Xu Y, Chen L, Li F, *et al.* Game-based event-triggered path-following optimal control of unmanned sailboats in sensor-to-controller channel. *Ocean Eng.* 2026, 358:125726.

[35] Liu L, Li X, Liu Y, Tong S. Neural network based adaptive event trigger control for a class of electromagnetic suspension systems. *Control Eng. Pract.* 2021, 106:104675.

[36] Liu Z, Shi P, Chen B, Lin C. Control design for uncertain switched nonlinear systems: adaptive neural approach. *IEEE Trans. Syst. Man Cybern.-Syst.* 2021, 51(4):2322–2331.

[37] Li Y, Yang G. Adaptive asymptotic tracking control of uncertain nonlinear systems with input quantization and actuator faults. *Automatic* 2016, 72:177–185.

[38] Deng Y, Zhang Z, Gong M, Ni T. Event-triggered asymptotic tracking control of underactuated ships with prescribed performance. *IEEE Trans. Intell. Transp. Syst.* 2023, 24(1):645–656.